Design and Control of a passive noise rejecting Variable Stiffness Actuator

Luca Fiorio[1], Francesco Romano[1], Alberto Parmiggiani[1], Bastien Berret[2,3], Giorgio Metta[1], Francesco Nori[1]

Abstract Inspired by the biomechanical and passive properties of human muscles, we present a novel actuator named passive noise rejecting Variable Stiffness Actuator (pnrVSA). For a single actuated joint, the proposed design adopts two motor-gear groups in an agonist-antagonist configuration coupled to the joint via serial non-linear springs. From a mechanical standpoint, the introduced novelty resides in two parallel non-linear springs connecting the internal motor-gear groups to the actuator frame. These additional elastic elements create a closed force path that mechanically attenuates the effects of external noise. We further explore the properties of this novel actuator by modeling the effect of gears static frictions on the output joint equilibrium position during the co-contraction of the agonist and antagonist side of the actuator. As a result, we found an analytical condition on the spring potential energies to guarantee that co-activation reduces the effect of friction on the joint equilibrium position. The design of an optimized set of springs respecting this condition leads to the construction of a prototype of our actuator. To conclude the work, we also present two control solutions that exploits the mechanical design of the actuator allowing to control both the joint stiffness and the joint equilibrium position.

1 Introduction

In the past decades industrial robotics has been the dominating sector in the robotic sales worldwide. However, there are indications that today's robotics market is about to undergo substantial changes. Recently, promising advances have been obtained

[1]The authors are with the iCub Facility department, Istituto Italiano di Tecnologia, 16163 Genova, Italy, e-mail: name.surname@iit.it
[2]The author is with the CIAMS, Univ. Paris-Sud, Universit Paris-Saclay, F-91405 Orsay, France , e-mail: name.surname@u-psud.fr
[3]The author is with the Institut Universitaire de France (IUF), France

in the emerging sector of "compliant robots", mostly from research laboratories and universities. Compliant robots are intended to interact with unstructured and dynamic environments. Possible application scenarios include human-robot interaction and collaboration, walking and running robots, prosthetic devices and exoskeletons, and more applications will probably be conceived as the sector grows.

The development of compliant robots has been possible thanks to the increment of processing power of digital controllers and the design of novel actuators.

The first compliant robots have been conceived by exploiting force sensors and classical stiff actuators, composed only by electric motors and gears. As an example, by exploiting accurate force measurements and fast control loops it has been possible to perform challenging interaction tasks, as reported by Albu-Schaffer and Hirzinger (2002).

However, there are intrinsic limitations to what the controller can do to modify the behavior of the system because inertia and friction play a dominant role in defining its bandwidth. To overcome this limitation, roboticists have developed a new set of systems endowed with an intrinsic (i.e. passive) compliance. From a mechanical standpoint, advances were closely tied to the development of new actuators that try to introduce at the mechanical level the advantages of compliance. Series Elastic Actuators (SEA), firstly introduced by Pratt and Williamson (1995), nowadays represent an established technology to drive robotic joints. To overcome the constant stiffness limitation of the SEA, several Variable Stiffness Actuators (VSA) have also been introduced more recently (see Vanderborght et al (2013) and Van Ham et al (2009)). Conceptually, as detailed in Table 1, the novel actuators differ from their stiff counterpart in the way joint compliance is achieved. However, joint position control is still achieved through active feedback (i.e. software feedback).

Relying on active feedback in artificial agents (such as humanoid robots) might not be a practical strategy to deal with external perturbations, specifically considering the growing amount of sensors (e.g., distributed force/torque sensors (see Fumagalli et al (2012)),whole-body distributed tactile sensors (see Del Prete et al (2012)), gyros and accelerometers (see Traversaro et al (2015))) which are currently available and have to be acquired and centrally processed to perform complex actions. Furthermore, closed-loop stability with respect to model inaccuracies or friction and backlash in transmissions, can be maintained under small delays in the feedback loop, while most closed loop systems become unstable for large delays.

In humans, the Central Nervous System (CNS) does not always rely on feedback loops to achieve an efficient trajectory control of limbs subject to environmental noise. Indeed, as described by Paillard (1996), our sensory feedback (visual or proprioceptive) is too slow. In this context, as described by Hogan (1984), one of the most interesting characteristics of biological actuators is the ability to passively compensate for external perturbations, without explicitly relying on active feedback. We name this feature *passive noise rejection* (*pnr*).

Starting from these premises, we propose a definition of passive noise rejecting VSA (pnrVSA) as the set of actuators that combine intrinsic compliance with the ability to passively compensate external disturbances (see Table 1). Furthermore we propose the design of a novel single-joint pnrVSA, based on four non-linear

Table 1 Comparison of position and compliance control method for different robotic actuators.

Actuator	Joint Position	Joint Compliance
Stiff Actuator	ACTIVE	ACTIVE
SEA / VSA	ACTIVE	PASSIVE
pnrVSA	PASSIVE	PASSIVE

springs and two electric motors in agonist-antagonist configuration. The distinguishing characteristic of the proposed mechanism is a closed force path that connects the actuator output joint to the actuator frame, allowing for the implementation of a passive mechanical feedback.

The work is organized as follows. Section 2 introduces the key mechanical features of a *pnr* design. Section 3 presents the "case study" prototype focusing on its main features, introduces the dynamical model of the actuator and the analytical description of the sensitivity of its internal states. We highlight the issue caused by the gear friction providing the mathematical representation of friction propagation among the actuator. Furthermore, we deduce which conditions the non-linear springs should satisfy to reduce the effects of gear friction. Section 4 introduces two different control strategies which exploit the peculiarities of the proposed device. Section 5 presents the results of the simulations together with the experimental tests to prove the effectiveness of the non-linear springs in reducing the effects of the gear friction.

2 Background

The design of a robotic manipulator that can reliably interact with an unstructured environment has to consider also impact loads and manipulation tasks in unstable force fields[1]. In such situations, the actuator has to provide the necessary force or torque to maintain the manipulator as close as possible to the desired trajectory. We define the activity of compensating for the errors in joint position due to external perturbations as "noise rejection". If we consider non-*pnr* actuators, this compensation task is completely entrusted to the digital controller (i.e. active feedback), while in *pnr* actuators part of this compensation is achieved thanks to the passive properties of the system.

[1] An example of unstable force field manipulation is represented by the task of keeping a screwdriver in the slot of a screw, as reported by Burdet et al (2001a).

2.1 Passive Noise Rejection Designs

To easily understand the difference between a *pnr* and a non-*pnr* design we can compare the mechanical structure of the two systems. Figure 1a represents a simplified model of a non-*pnr* actuator using a linear motor. The motor (ϑ) is linked to the joint (q) through a transmission and a variable stiffness spring (c). This elastic element in between the transmission and the joint is the key component of a typical VSA[2]. As observed before, a disturbance that affects the position of the joint can be compensated only by relying on the motor through active feedback. Depending on the feedback delay and on the frequency and amplitude of the external perturbation, Berret et al (2011) have shown that the system can become unstable.

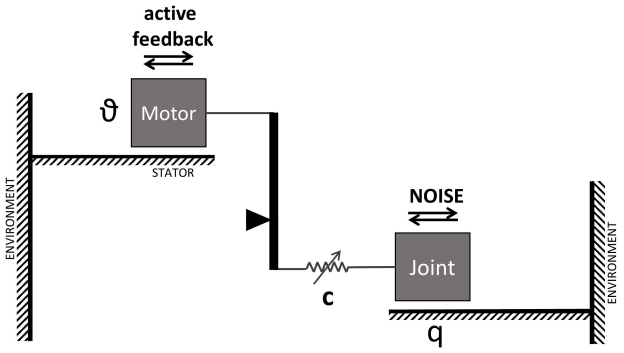

(a) Classic VSA

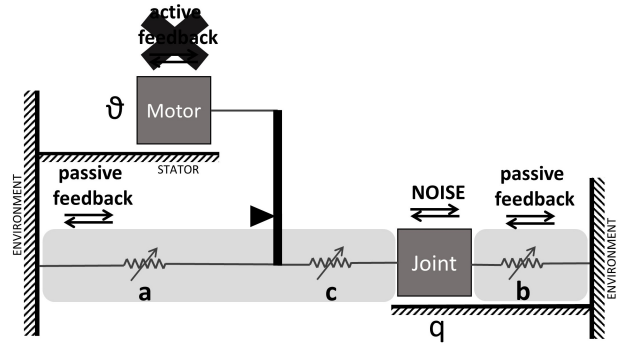

(b) pnrVSA

Fig. 1 Conceptual design of an actuation system using a linear motor. (a) Schematic representation of a classical VSA. (b) Generic representation of a pnrVSA. The components a, b and c represent the elastic elements, while ϑ and q represent the motor and the joint respectively.

[2] The same model can represent a classical SEA by using a constant stiffness spring, or a stiff actuator by removing the spring and connecting the joint directly to the transmission

Figure 1b represents instead a simplified model of a *pnr* actuator. The spring elements connecting the joint to the environment, a and b, are typically not present in non-*pnr* designs. Nevertheless, they play a crucial role in determining the overall system passive noise rejection. In practice when $a = b = 0$ the system is free-floating with respect to the environment, and noise can drive the system arbitrarily far from the target configuration. The advantage given by the spring elements a and b resides in the closed loop paths that connect the joint directly to a fixed frame (i.e. the actuator frame). Thanks to one of these paths, either $frame - a - c - joint$ or $frame - b - joint$, the joint has a unique equilibrium position. In this case, when an external perturbation deviates the joint from its equilibrium position the elastic elements generate a passive restoring force.

In a work by Berret et al (2012), we studied the effect of disturbances acting on a *pnr* actuator. Disturbance has been represented by stochastic variables acting as forces on the joint. Computations showed that the passive noise rejection monotonically increases with the stiffness of the elastic elements a, b and c. In a sense, passive noise rejection is increased by augmenting the stiffness of the path that connects the joint to the fixed frame. Indeed, the mechanical bandwidth of the connection is closely related to the passive noise rejection: the higher the bandwidth the faster the passive response (meant as the restoring force) of the system. In this sense, the most important advantage of the mechanical feedback is that feedback happens physically without the typical delays of active control loops.

In this work, we focus on actuators like the ones in Fig. 1b, i.e. not having a and b simultaneously zero.

2.2 Agonist-antagonist design

The agonist-antagonist arrangement is a design suitable to construct a *pnr* actuator. As seen in the introduction, a nice example of agonist-antagonist system with *pnr* is given by the human actuation model. In particular, muscles arranged in antagonistic pairs create two closed paths that connect the joint (the limb) to a fixed frame (the previous limb).

The main properties of the biological muscles have been reported by Hill and Gasser (1924) using the model represented in Figure 2 (a), used to model the tension dynamics of various isolated frog muscles. It can be proven (see McMahon (1984) pag.23) that its mechanical model is equivalent to the one shown in Figure 2 (b) and therefore the overall muscle force can be written as:

$$F = F_{SE}(K_{SE}, l_2) = F_{PE}(K_{PE}, l_1) + P(L_j, f(t)),$$

where K_{SE} is the series nonlinear elastic element, K_{PE} is the parallel nonlinear elastic element, which in series with K_{SE} account for the passive tension properties of the muscle, and P is the active force generated by the contractile element depending on the muscle history activation $f(t)$ and the overall length L_j. Indeed, biological

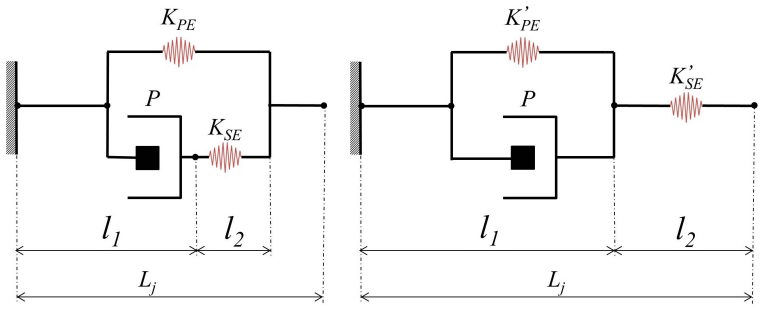

(a) Hill muscle model (b) Equivalent muscle model

Fig. 2 Mechanical circuit diagrams showing two equivalent muscle models. Source (Nori et al (2012))

muscles behave both as unidirectional force sources and non-linear springs, and, consequently, thanks to the agonist-antagonist arrangement, the joint has a unique equilibrium position that depends on the "co-contraction" level of the agonist and antagonist muscles. When a disturbance deviates the joint from its equilibrium position, the muscles thanks to their passive elastic properties generate a restoring force that compensates for the external disturbance. Nevertheless, the limited stiffness of tendons and muscles puts some bounds on the joint stiffness that can be achieved in humans. In support to this analysis, different research studies analyzed the relationship between the joint passive properties and human motor control (see De Luca and Mambrito (1987), Polit and Bizzi (1979) and Burdet et al (2001b)).

When we consider robotic actuators, different agonist-antagonist actuator designs have been presented in literature. In general, as described by Migliore et al (2005), two internal motors act on the same joint through non-linear springs. Concordant actuation of the internal motors causes only the displacement of the output joint, while opposite actuation determines a pure joint stiffness variation. Other examples, include the quasi-antagonistic design described by Eiberger et al (2010), the bidirectional design described by Petit et al (2010) and the cross-coupled design described by Tonietti et al (2005) and Schiavi et al (2008). Nevertheless, the majority of these designs belong to the category of classical VSA, while only few possess also the *pnr* property. As an example, Bicchi et al (2002) propose a one degree of freedom joint driven by means of two artificial muscles which, similarly to the biological counterparts, create two closed paths connecting the joint to the actuator frame. The NeurArm described by Vitiello et al (2007) instead, is a two degrees of freedom planar robotic arm specifically designed and developed for investigating models of human motor control principles and learning strategies.

To the best of our knowledge, however, a design based on rotary actuators which are more commonly employed when designing robotics arms, has not been proposed yet.

3 Actuator Design

Conventional agonist-antagonist systems are constituted by two actuation modules arranged symmetrically around the output joint. In our case, the design problem to be solved was to conceive a module possessing the *pnr* property, and that could have been arranged in an antagonist configuration. With reference to Figure 1 we can identify the key mechanical components of this module considering a, ϑ and c. The complete design is described in the following sections, where details on a specific pnrVSA implementation are given.

3.1 Conceptual Design

As shown in Figure 3 we followed a design based on non-linear springs (red coiled elements) which can vary their equilibrium configuration thanks to the agonist-antagonist arrangement. The springs are connected through wires (red lines) to the actuator output joint q, the actuator frame and to the motor capstans ϑ and ϑ^a. Within a module, each spring has a different behavior when the motor capstan rotates. The spring connecting the capstan to the frame, named K_{PE}, works in parallel with respect to the capstan (spring elongation is proportional to capstan angular displacement); the spring K_{SE} connecting the capstan to the output joint, instead, behaves as series elastic element.

Considering the whole system, we can describe the behavior of the output joint with respect to angular displacements of both capstans. Intuitively, a clockwise rotation of the capstan ϑ coupled with the same counterclockwise rotation of ϑ^a stretches all springs causing no movement of the joint q. Conversely, rotating the two capstans in the same clockwise direction results into a pure movement of the joint without affecting its stiffness.

3.2 Analytical Model and Analysis

In the following section, we describe the analytical model of the proposed *pnr*VSA. Subsequently, the model is used to describe the main properties of the system.

3.2.1 Notation

With reference to the actuator schema in Figure 3, we define the following quantities:

- ϑ and ϑ^a represent the angular position of the agonist and antagonist capstans, τ_ϑ and τ_ϑ^a are the associated torques.

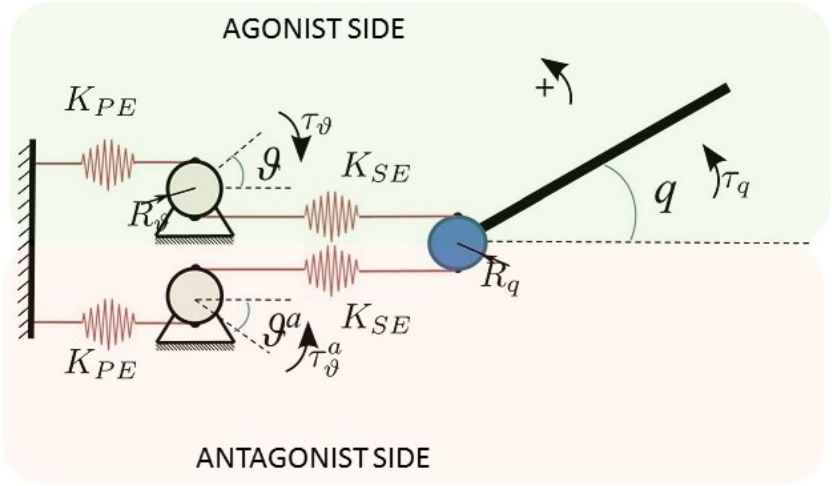

Fig. 3 pnrVSA prototype diagram: the output joint q is controlled by means of internal actuation torques τ_ϑ and τ^a_ϑ, while ϑ and ϑ^a represent capstan angular positions. τ_q is an external torque acting on the output joint.

- q is the joint position, τ_q the associated torque.
- I_ϑ is the inertia of the capstan and R_ϑ its radius.
- I_q is the joint inertia and R_q is the radius of the joint pulley.
- U_{PE} represents the potential energy of the parallel springs[3]. We named U_1 the agonist parallel spring and U_4 the antagonist one.
- U_{SE} represents the potential energy of the series springs. We named U_2 the agonist serial spring and U_3 the antagonist one.
- $l_i, i = 1,\dots,4$ is the spring elongation for the i-th spring, i.e.:

$$
\begin{aligned}
l_1 &= -R_\vartheta\,\vartheta \\
l_2 &= -R_\vartheta\,\vartheta - R_q q \\
l_3 &= R_\vartheta\,\vartheta^a + R_q q \\
l_4 &= R_\vartheta\,\vartheta^a
\end{aligned}
$$

We also use the following notation throughout the rest of the paper:

- Given a time function $f(t) \in \mathbb{R}^n$, the first and second order time derivatives are denoted by $\dot{f}(t)$ and $\ddot{f}(t)$, respectively.
- Given a function $f(x)$, we denote the first, second and third order derivatives with respect to its argument by $f'(x) = \frac{\partial f}{\partial x}$, $f''(x) = \frac{\partial^2 f}{\partial x^2}$ and $f'''(x) = \frac{\partial^3 f}{\partial x^3}$,

[3] To make the analysis as general as possible, the non-linear spring potential energies are kept unspecified in the theoretical analysis.

respectively. When the function argument is clear, we will use the "prime" notation, for sake of conciseness.

- Given the angular position variables and the associated torques, for the sake of notational simplicity, we define:

$$\hat{\vartheta} := -R_{\vartheta}\,\vartheta$$

$$\hat{\vartheta}^a := R_{\vartheta^a}\,\vartheta^a$$

$$\hat{q} := -R_q q$$

$$\hat{\tau}_{\vartheta} := \frac{\tau_{\vartheta}}{R_{\vartheta}}$$

$$\hat{\tau}_{\vartheta^a} := \frac{\tau_{\vartheta^a}}{R_{\vartheta^a}}$$

$$\hat{\tau}_q := \frac{\tau_q}{R_q}$$

3.2.2 System Modeling

The dynamical model of the mechanical system can be written by using the Euler-Lagrange formulation:

$$\begin{cases} I_{\vartheta}\,\ddot{\vartheta} - R_{\vartheta}\frac{\partial U_1}{\partial l_1}(-R_{\vartheta}\,\vartheta) - R_{\vartheta}\frac{\partial U_2}{\partial l_2}(-R_{\vartheta}\,\vartheta - R_q q) = \tau_{\vartheta} \\ I_{\vartheta^a}\,\ddot{\vartheta}^a + R_{\vartheta^a}\frac{\partial U_4}{\partial l_4}(R_{\vartheta^a}\,\vartheta^a) + R_{\vartheta^a}\frac{\partial U_3}{\partial l_3}(R_{\vartheta^a}\,\vartheta^a + R_q q) = \tau_{\vartheta^a} \\ I_q\ddot{q} - R_q\frac{\partial U_2}{\partial l_2}(-R_{\vartheta}\,\vartheta - R_q q) + R_q\frac{\partial U_3}{\partial l_3}(R_{\vartheta^a}\,\vartheta^a + R_q q) = \tau_q. \end{cases} \tag{1}$$

The state of the mechanism is thus $x := \begin{bmatrix} \vartheta & \vartheta^a & q & \dot{\vartheta} & \dot{\vartheta}^a & \dot{q} \end{bmatrix}^\top$, and we are interested in controlling the joint position variable q. It is worth noting that the torque applied at the joint side τ_q, for which no direct control is available, has to be interpreted as an **external disturbing torque**. On the other hand, the torques applied at the agonist τ_{ϑ} and antagonist τ_{ϑ^a} sides of the actuator represent the **internal actuation torques**.

Given an equilibrium configuration $x_{\text{eq}} = \begin{bmatrix} \vartheta_{\text{eq}} & \vartheta^a_{\text{eq}} & q_{\text{eq}} & 0 & 0 & 0 \end{bmatrix}^\top$, the torques must satisfy the following equation:

$$\begin{cases} -U_1'(\hat{\vartheta}) - U_2'(\hat{\vartheta} + \hat{q}) = \hat{\tau}_{\vartheta} \\ U_4'(\hat{\vartheta}^a) + U_3'(-\hat{q} + \hat{\vartheta}^a) = \hat{\tau}_{\vartheta^a} \\ -U_2'(\hat{\vartheta} + \hat{q}) + U_3'(-\hat{q} + \hat{\vartheta}^a) = \hat{\tau}_q, \end{cases} \tag{2}$$

where we adopted the "hat" and prime notation for the sake of simplicity.

Definition 1 Given the system (1), we define **co-contraction** as the control action that satisfies:

$$\dot{\hat{\vartheta}} > 0,$$
$$\dot{\hat{\vartheta}}^a > 0.$$

As seen in Section 3.1, this control action stretches all the springs.

Definition 2 Considering the vector of the actuator internal/external torques $\tau = \left[\hat{\tau}_\vartheta, \hat{\tau}_{\vartheta^a}, \hat{\tau}_q\right]^\top$ and the vector of the capstan/joint position $\alpha = \left[\hat{\vartheta}, \hat{\vartheta}^a, \hat{q}\right]^\top$, by exploiting the implicit function theorem, we define as **sensitivity matrix** the Jacobian matrix (see the Appendix 6.1 for the complete matrix):

$$\frac{\partial \alpha}{\partial \tau} = \begin{bmatrix} \frac{\partial \hat{\vartheta}}{\partial \hat{\tau}_\vartheta} & \frac{\partial \hat{\vartheta}}{\partial \hat{\tau}_{\vartheta^a}} & \frac{\partial \hat{\vartheta}}{\partial \hat{\tau}_q} \\ \frac{\partial \hat{\vartheta}^a}{\partial \hat{\tau}_\vartheta} & \frac{\partial \hat{\vartheta}^a}{\partial \hat{\tau}_{\vartheta^a}} & \frac{\partial \hat{\vartheta}^a}{\partial \hat{\tau}_q} \\ \frac{\partial \hat{q}}{\partial \hat{\tau}_\vartheta} & \frac{\partial \hat{q}}{\partial \hat{\tau}_{\vartheta^a}} & \frac{\partial \hat{q}}{\partial \hat{\tau}_q} \end{bmatrix}. \tag{3}$$

The analytical expression of $\partial\alpha/\partial\tau$ will play a crucial role in Section 3.3 during the modeling of the effects of stiction on the output joint q. In particular, we will focus on the quantities referred to the sensitivity of the output joint to the internal actuation torques $\frac{\partial \hat{q}}{\partial \hat{\tau}_\vartheta}$ and $\frac{\partial \hat{q}}{\partial \hat{\tau}^a_\vartheta}$, aiming at characterizing how the equilibrium configuration for q is affected by static friction acting on ϑ and ϑ^a.

The analytical expression for $\partial\alpha/\partial\tau$ will also play a major role in Section 4. In particular, it will be used to design a control policy that maintains the joint equilibrium configuration and regulates the actuator intrinsic stiffness.

3.2.3 System Properties

We now state two important properties of the considered system, together with the sufficient conditions to hold, when co-contracting control actions are used.

Proposition 1 Suppose a control action satisfies Definition 1, that is, it is a co-contracting control action. If the springs are designed such that holds:

$$U_i'' > 0$$
$$U_i''' > 0$$

with

$$i = 1, \ldots, 4,$$

then, the control action is increasing the individual stiffness of each spring. As a consequence, $\frac{\partial \hat{\tau}_q}{\partial \hat{q}}$, i.e. the joint level stiffness, is monotonically increasing.

We compute the joint level stiffness, defined as the sensitivity of the equilibrium configuration $\hat{q}$ with respect to variations of the external torque $\hat{\tau}q$. Analytically, this quantity coincides with $\partial\hat{q}/\partial\hat{\tau}_q$ and therefore it can be extracted as the element $(3,3)$ in the matrix $\partial\alpha/\partial\tau$:

$$\frac{\partial\hat{q}}{\partial\hat{\tau}_q} = -\frac{U_1''U_2''U_3'' + U_1''U_2''U_4'' + U_3''U_4''U_1'' + U_1''U_3''U_4''}{(U_1''+U_2'')(U_3''+U_4'')}.$$

Easy calculations show that we have:

$$\frac{\partial\hat{q}}{\partial\hat{\tau}_q} = -\frac{1}{\frac{1}{\frac{1}{U_1''}+\frac{1}{U_2''}} + \frac{1}{\frac{1}{U_3''}+\frac{1}{U_4''}}}.$$

This last equation represents the intuitive result that the joint stiffness is the series of parallel of springs, nominally the series of U_1, U_2 in parallel with the series of U_3, U_4. It is indeed intuitive to conclude that global stiffness will increase if all individual stiffnesses (U_1, U_2, U_3, U_4) are increased.

At the control level, this is a desirable property because increasing the joint stiffness increases also the actuator *pnr*.

We now focus our attention on the quantity $\partial\hat{q}/\partial\hat{\tau}_\vartheta$ which represents the sensitivity of the joint position $\hat{q}$ with respect to the internal torque $\hat{\tau}_\vartheta$. Thanks to the symmetry of the system, the properties hereafter discussed will hold for the analogous quantity $\partial\hat{q}/\partial\hat{\tau}_{\vartheta^a}$.

Proposition 2 Suppose a control action satisfies Definition 1, that is, it is a co-contracting control action. If the parallel and series springs are selected such that

$$\frac{U_1''}{U_1'''} < \frac{U_2''}{U_2'''}$$

holds, then, the control action leads to decreasing value of $\partial\hat{q}/\partial\hat{\tau}_\vartheta$.

From the expression of $\partial\alpha/\partial\tau$, we have:

$$\frac{\partial\hat{q}}{\partial\hat{\tau}_\vartheta} = \frac{U_2''}{U_1''+U_2''}\frac{\partial\hat{q}}{\partial\hat{\tau}_q},$$

and inverting the expression above we have:

$$\left(\frac{\partial\hat{q}}{\partial\hat{\tau}_\vartheta}\right)^{-1} = \underbrace{\frac{U_1''+U_2''}{U_2''}}_{g(\hat{\vartheta},\hat{q})} \underbrace{\left(\frac{\partial\hat{q}}{\partial\hat{\tau}_q}\right)^{-1}}_{\text{joint stiffness}}. \tag{4}$$

From Equation (4), we notice that this property is guaranteed if both the joint stiffness and the function $g(\vartheta,q)$ are increasing. From *Proposition* 1, we already know

that the joint stiffness is increasing under the selected control action. Therefore we are left with guaranteeing that $g(\hat{\vartheta},\hat{q})$ is non-decreasing in $\hat{\vartheta}$.

Easy computations show that:

$$\frac{\partial g}{\partial \hat{\vartheta}} > 0 \qquad \Longleftrightarrow \qquad \frac{U_1''}{U_1'''} < \frac{U_2''}{U_2'''}.$$

At the control level, this is a desirable property because it allows to have finer control over the variable $\hat{q}$ (since identical variations in the control variables τ_ϑ, τ^a_ϑ will correspond to smaller variations in the equilibrium configuration for $\hat{q}$).

3.3 Stiction Compensation

Static friction, due to its discontinuous nature, can produce undesired behaviors that are rather difficult to compensate. In particular, with reference to agonist-antagonist VSA, friction is often identified as one of the most evident and most adverse drawbacks. All antagonistic actuators are based on the primary idea of co-contracting both agonist and antagonist motor sides of the system to increase joint stiffness. As a consequence, internal forces increase. Among internal forces we have also friction and stiction components that, due to their non-linear nature, greatly degrade the performance of the antagonistic actuators. This decay in performance is, together with inertia issues, a limit for controlling the actuator mechanical bandwidth while performing torque control or dynamic tasks involving human or environment interaction. Different approaches have been proposed to reduce these drawbacks. As an example, we have classical integrator, action and disturbance observer described by de Wit et al (1994), adaptive controllers described by Tomei (2000), sliding mode control described by Parra-Vega and Arimoto (1996) or model-based friction compensation described by Armstrong (1988) and Bona and Indri (2005). All of these approaches have the advantage of being fast and accurate, but most of them reduce the benefit of inherent passive compliance to a certain extent. Controllers indeed introduce an additional compliance which acts upon the series, variable or fixed, elasticity and that could be difficult to tune.

As we have seen in Section 2.1, one of the key features of the pnrVSA is the unique equilibrium position of its output joint. However the presence of static friction[4] gives rise to a set of "indifferent" equilibrium configurations. This range of equilibrium positions, named "dead-band" $\triangle q$, rapidly increases together with actuator co-contraction. To understand this behavior we can imagine that when the output joint q is displaced from its unique equilibrium position, the synergistic action of the two closed path (K_{PE} + K_{SE} for both the agonist and the antagonist modules) should generate a restoring force. In our system this behavior is abated because the gear stiction prevents the rotation of the capstans.

[4] In our actuator the main source of static friction are the gearboxes that have been used to connect the electric motors to the capstans (see Figure 4).

Starting from the observation that both friction and spring restoring forces can be represented as a function of the actuator internal forces, we explored the possibility of mechanically compensating stiction's adverse effects by exploiting the actuator elastic elements. We derived one analytical condition over the potential energy of the elastic elements to ensure that during co-contraction the increase of the spring restoring forces is "greater" than the increase of the friction forces.

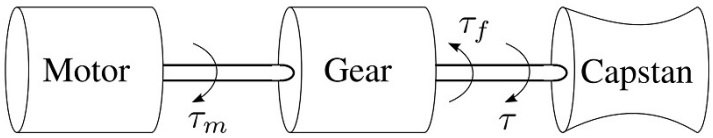

Fig. 4 The picture shows the motor subsystem: the motor is connected to the capstan by the gear. Friction effects between gear teeth greatly influence the torque transmission from motor to gear and vice-versa. Source (Fiorio et al (2013)).

As described by Fiorio et al (2014), to perform our qualitative analysis we assumed that the torque due to static friction is a function of the torque acting on the capstan[5]: $\tau_f = \tau_f(\tau)$, with τ being either τ_ϑ or τ_{ϑ^a} depending on the considered capstan. The analytical description of the dead-band can then be found considering the sensitivity matrix defined in Equation 3. In particular, we can think of the dead-band as the consequence of an uncertainty that affects the torques that are applied at the capstans, where the amplitude of this uncertainty can be represented by the stiction torque. In this perspective, the total actuator dead-band $\triangle q$ can be seen as the sum of the contributions coming from the agonist and antagonist side, yielding:

$$\triangle q = \frac{\partial \hat{q}}{\partial \hat{\tau}_\vartheta} \hat{\tau}_f(\hat{\tau}_\vartheta) + \frac{\partial \hat{q}}{\partial \hat{\tau}_{\vartheta^a}} \hat{\tau}_f^a(\hat{\tau}_{\vartheta^a}) \ . \tag{5}$$

Equation 5 analytically defines the global actuator dead-band as a function of the internal system torques (and thus the co-contraction level), and describes how the static friction on the gearbox is reflected on the output joint.

To guarantee that co-contraction reduces the effect of gearbox friction on the joint equilibrium position, we formulated a differential condition on the spring potential energies. To make the analysis as general as possible, the conditions were expressed by assuming a generic functional dependence between stiction τ_f and applied torque τ. Similarly the non-linear spring potential energies were kept unspecified. We then studied how Equation (5) varies with variations of $\hat{\tau}_\vartheta$ and $\hat{\tau}_{\vartheta^a}$. The major outcome of this analysis is the condition in order for the dead-band Δq to decrease with co-contraction:

$$\frac{\partial}{\partial \hat{\tau}_\vartheta} \left(\frac{U''_{SE}}{U''_{SE} + U''_{PE}} \hat{\tau}_f \right) < 0 \ . \tag{6}$$

[5] This assumption derives from the fact that co-activation increases internal forces. Certain friction forces, such as stiction, increase with gear teeth normal forces and therefore an increased stiction should be expected in response to an increased level of internal forces.

If the potential energies of the parallel and series spring are selected such that condition (6) is satisfied, we are guaranteed that during co-contraction the deadband decreases instead of increasing. This is a significant result because it shows that it is possible to passively compensate the increase of static friction. In other words, this improvement in the actuator design adds a passive property that accomplishes a control objective mechanically.

3.4 Embodiment Design

In this section we present an overview of the actuator mechanical design focusing on the non-linear springs. The design process and the actuator performances have been extensively reported by Fiorio et al (2012).

3.4.1 Non-linear spring design

The final actuator design includes the four non-linear springs whose force-displacement characteristic has been optimized and customized in order to have light and compact solutions for both the parallel elastic element K_{PE} and the series elastic element K_{SE}. The differential inequality of Equation 6 has been solved analytically. For this purpose we considered the condition as a single functional of $\hat{\tau}_\vartheta$ relating the potential energy of both springs to each other. With this approach we solved the differential inequality and made explicit the relation between serial and parallel elastic elements. Eventually, the analytical solution has been optimized for our setup by relying on a numerical optimization. The construction of an optimized set of springs, respecting these conditions, led to the construction of a version of our actuator which showed that for increasing levels of co-contraction the effect of stiction, and thus the dead-band effect, decreases (see tests in Section 5). Figure 5 shows the force-displacement functions of the non-linear springs that have been designed complying with condition (6).

To construct the non-linear springs, we exploited the idea of "non-circular spool", where the change in stiffness is achieved through a cam of varying radius, specialized into two different custom solutions. Regarding the K_{SE} spring a steel cable is wound around a non-circular spool in parallel to a linear torsional spring. Figure 6 shows a model of the non-linear spring. For the parallel elastic element K_{PE} we had to consider that due to the wide range of motion of the output joint, its non-circular spool performs more than one rotation and has been therefore realized with a three-dimensional cut of the non-circular profile. Furthermore, in order to reduce the total spring size, the design has been optimized connecting directly the motor shaft to the non-circular spool. A steel cable connected to a linear compression spring is then wound on the non-circular spool (see Figure 7 (b)). The complete actuator CAD is shown in Figure 7 (a), while in Figure 8 the shape of both the non-circular spools is depicted.

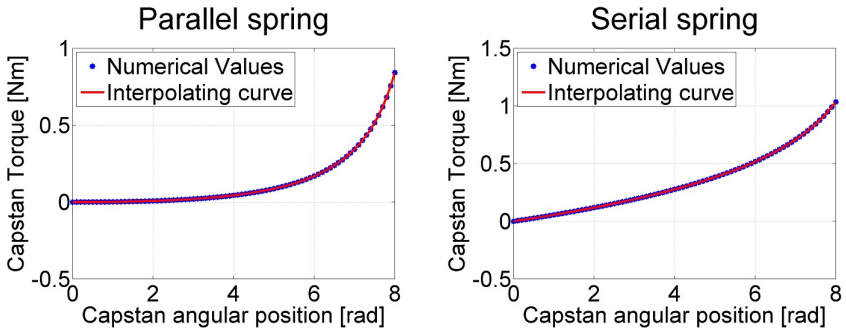

Fig. 5 The plots show the non-linear force-displacement characteristics of the parallel and series springs. The characteristics have been computed through a numerical optimization. Source (Fiorio et al (2014))

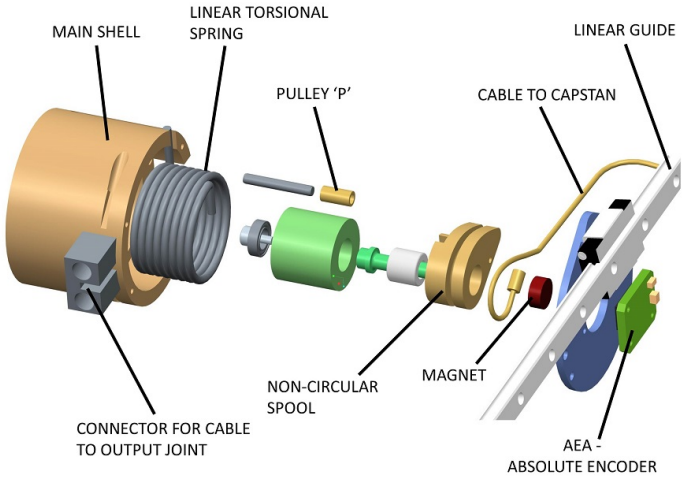

Fig. 6 The exploded view of the K_{SE} elastic element, which can be seen as a non-linear extensional spring.

3.4.2 Actuator construction

The actuator has been constructed using aluminum for most of its components. In particular we used "ERGAL 7075-T6 temper" alloy. We selected this material because it has a low density (2810 $[kg/m^3]$), good mechanical properties (ultimate tensile strength of 510-540 $[MPa]$) and can be easily machined using Computer Numerical Control (CNC) machines. Only for some critical components we had to use a more robust material. In particular, all the non-circular spools and some other components of the non-linear springs were made with the stainless steel "17-4 PH". Another interesting peculiarity of the non-circular spools is that, due to their complex shape, some of them have been manufactured using Selective Laser Sin-

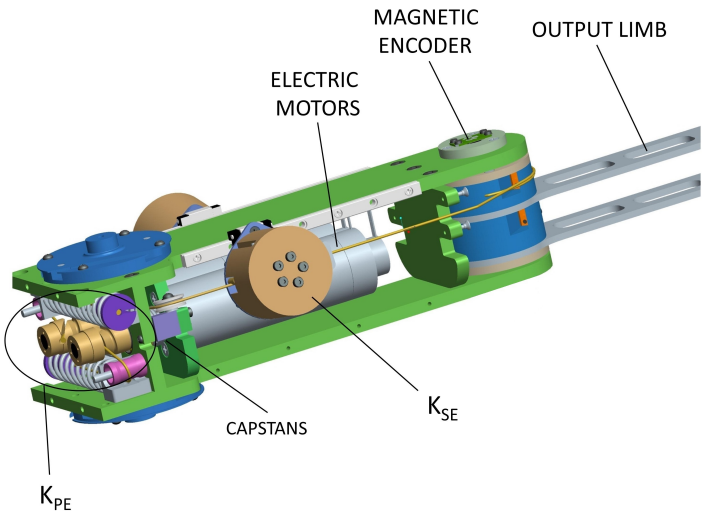

(a) Complete assembly

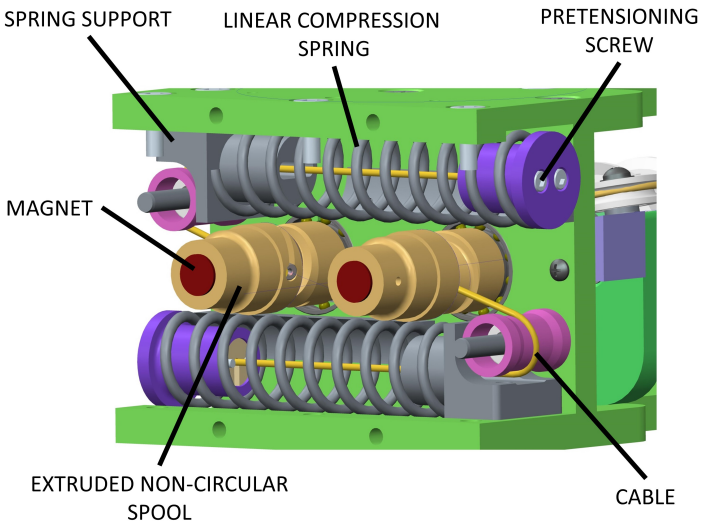

(b) K_{PE} design

Fig. 7 In figure (a), the complete assembly: the two electric motors are connected, through their relative gears, to the capstans. Each capstan winds the cable (yellow) that stretches the K_{SE} springs. In figure (b), a detailed view of how the parallel elastic elements have been integrated directly on the motor shaft: the extruded non-circular spools, that realize the parallel elastic elements K_{PE}, are fastened together with the capstans on the motor shafts. The pretensioning screws are used to align the capstans with the zero configuration (i.e. all springs elongations are zero). Source (Fiorio et al (2012)).

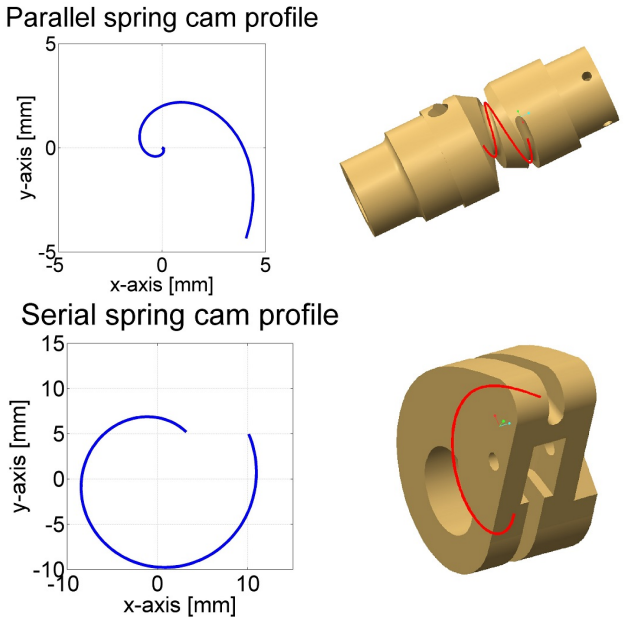

Fig. 8 The plots show the profiles of the non-circular cams together with the CAD models of the spools. The non-circular profiles have been used to design the cable grooves. In particular due to the overlap in the profile of the parallel spring we had to design the spool extruding the cable groove in 3D.

tering (SLS). This technique is an additive manufacturing technology that uses the laser as a power source to melt powdered material to create a solid structure. All the mechanical connections between springs, frame, capstans and pulleys have been realized through steel cables. Figure 9 from *a* to *d* shows the 3D printed components and the assembled series and parallel springs. At the bottom (*e*) the complete actuator is shown.

4 Controller Design

In this section we describe two different control solutions that exploit the properties of the proposed passive noise rejecting variable stiffness actuator. In particular, we first design a control law capable of decoupling the regulation of the joint-stiffness from the joint equilibrium configuration (see also Nori et al (2012)). To test the passive noise rejecting property of the actuator, we also design a second type of control action. In particular, we formulate a Stochastic Optimal Control (SOC) problem (see also Romano et al (2014); Berret et al (2013)), and we apply the obtained control policy as a purely open-loop action, leaving to the actuator the responsibility of rejecting eventual disturbances. The main advantage of the SOC (Kappen

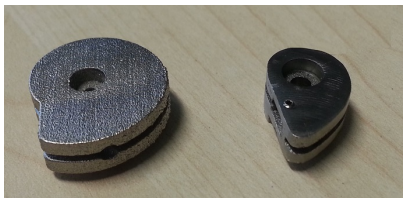

(a) Series spring - spool

(b) Parallel spring - spool

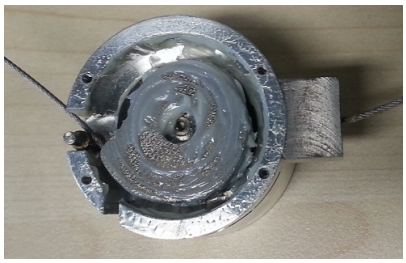

(c) Series spring assembled

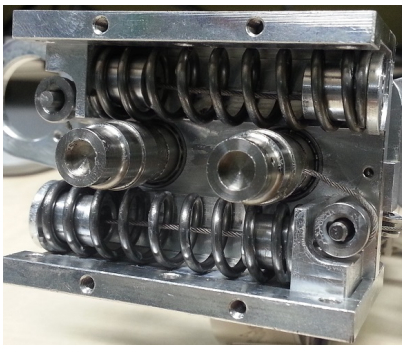

(d) Parallel springs assembled

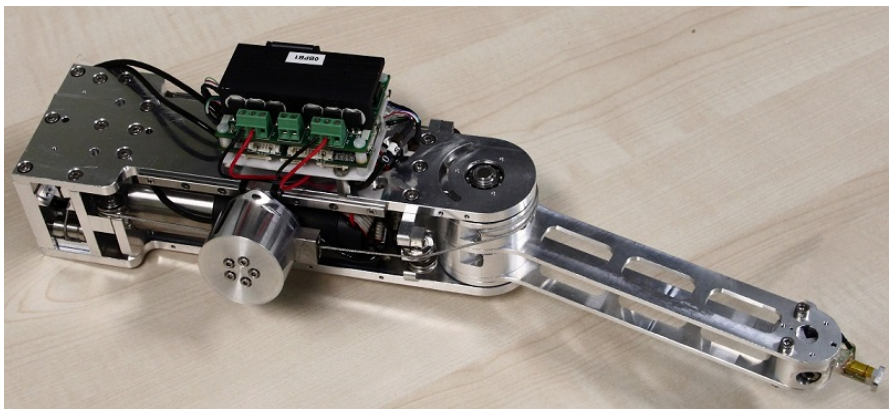

(e) Complete pnrVSA assembled

Fig. 9 From *a* to *d* some of the components of the actuator are shown, while at the bottom the complete actuator is depicted. In the pictures (*a*) and (*b*) it is possible to see a comparison between the coarse metal printed component and the finished one.

(2011)) strategy is the possibility to generate a complete motor plan characterized by a "global" perspective. In particular, this motor plan, is the optimal solution with respect to some optimization criteria, while taking into account stochastic information due to noise. End-effector positioning accuracy and energy consumption are just an example of possible optimization criteria that can be specified to the control problem. The latter, is of paramount importance due to the fact that co-contraction is energetically expensive, i.e. it is important to find the minimum level of co-contraction necessary to achieve the task.

Nevertheless, it is important to notice that both controllers generate "open-loop" solutions which fully exploit the native noise-rejection property of the actuator, without the need to rely on state estimations and feedback gains during control.

4.1 Stiffness and Position Control

The control action is computed considering the time derivative of the output joint position. Given that we do not have direct control on $\hat{\tau}_q$, assume that $\dot{\hat{\tau}}_q = 0$ so that the time derivative of $\hat{q}$ results to be:

$$\dot{\hat{q}} = \underbrace{\begin{bmatrix} \frac{\partial \hat{q}}{\partial \hat{\tau}_\vartheta} & \frac{\partial \hat{q}}{\partial \hat{\tau}_{\vartheta^a}} & \frac{\partial \hat{q}}{\partial \hat{\tau}_q} \end{bmatrix}}_{N} \underbrace{\begin{bmatrix} \dot{\hat{\tau}}_\vartheta \\ \dot{\hat{\tau}}_{\vartheta^a} \\ 0 \end{bmatrix}}_{\delta\tau}, \tag{7}$$

where $\delta\tau$ is the time derivative of the variable τ introduced by *Definition* 2, i.e. $\delta\tau = \dot{\tau}$, while an analytical expression for N is given by the last row of the sensitivity matrix (3). The generic solution of this control problem (imposing, as usual, direct control only on the internal torques) is given by the following:

$$\delta\tau = \begin{bmatrix} U_2''(U_3'' + U_4'') \\ U_3''(U_1'' + U_2'') \\ 0 \end{bmatrix} \cdot k_1 \cdot v + \begin{bmatrix} -U_3''(U_1'' + U_2'') \\ U_2''(U_3'' + U_4'') \\ 0 \end{bmatrix} \cdot k_2 \cdot u, \tag{8}$$

with:

$$\begin{aligned} k_2 &= U_1''U_2''U_3'' + U_1''U_2''U_4'' + U_1''U_3''U_4'' + U_2''U_3''U_4'', \\ k_1 &= k_2^2 \left(\left(U_2'' \left(U_3'' + U_4'' \right) \right)^2 + \left(U_3'' \left(U_1'' + U_2'' \right) \right)^2 \right). \end{aligned}$$

The control action $\delta\tau$ in Eq. (8) is composed of two terms. The first term, parametrized by the free variable $v \in \mathbb{R}$, acts directly on the time derivative of $\hat{q}$, i.e. is responsible of changing the equilibrium configuration of the output joint. The second variable $u \in \mathbb{R}$, instead, monotonically changes the joint stiffness while maintaining a constant value for $\hat{q}$, i.e.

$$\dot{\hat{q}} = N\,\delta\tau\Big|_{v=0} = 0, \quad \forall u \in \mathbb{R}.$$

4.2 Stochastic optimal control (SOC)

In the second control strategy we consider a stochastic non-linear control-affine system:

$$\mathrm{d}\mathbf{x} = \mathbf{a}(\mathbf{x}(t),t)\,\mathrm{d}t + B(\mathbf{x}(t),t)\mathbf{u}(\mathbf{x}(t),t)\,\mathrm{d}t + C(\mathbf{x},t)\,\mathrm{d}\mathbf{w}, \tag{9}$$

where $\mathbf{x} \in \mathbb{R}^n$ is the state of the system, $\mathbf{u} \in \mathbb{R}^m$ is the control input, $\mathbf{w} \in \mathbb{R}^m$ is brownian noise, $\mathbf{a}(\cdot)$ is the drift term, $B(\cdot)$ is the control matrix and $C(\cdot)$ is the diffusion matrix.

We also define the cost-to-go at time t_0, state $\boldsymbol{x}_0$ as:

$$J(\boldsymbol{x}_0,t_0) = \mathbb{E}[\phi(\boldsymbol{x}(t_f)) + \int_{t_0}^{t_f} \mathscr{L}(\boldsymbol{x},t) + \frac{1}{2}\boldsymbol{u}^\top R\boldsymbol{u}\,\mathrm{d}t], \tag{10}$$

where $\phi(\cdot)$ is a final state-dependent cost and $\mathscr{L}(\cdot)$ is the running cost term and $\mathbb{E}$ is the expected value operation.

The optimal cost-to-go J^* must satisfy the stochastic version of the Hamilton-Jacobi-Bellman (HJB) equation, which is a second order non-linear partial differential equation. The resulting optimal control $\boldsymbol{u}^*$ can then be expressed as

$$\boldsymbol{u}^* = -R^{-1}B^\top \frac{\partial J^*(\boldsymbol{x},t)}{\partial \boldsymbol{x}}. \tag{11}$$

The HJB equation can be transformed into a linear second order partial differential equation by performing a logarithmic transformation, $\psi = exp(\frac{1}{\lambda}J)$ and by assuming that $C = B\sqrt{\lambda R^{-1}}$, see Theodorou et al (2010). It can then be shown that the optimal control can be expressed at each state/time as a path integral which can be approximated via importance sampling methods.

It is worth noting that the control action in Eq. (11) is a state feedback action. In order to test the passive noise rejecting capabilities of the proposed actuator, we deliberately modify the control action to result in a pure open-loop action. It is thus responsibility of the noise rejecting property of the mechanism to ensure robustness against external disturbances.

5 Simulations and Experimental Tests

5.1 Spring Design Validation

To validate the non-linear spring design of Section 3.3 we tested the actuator with two different sets of series and parallel springs. The first set, named “optimized”,

has been designed complying with the condition (6), while the second set, named "quadratic", comprises two non-linear springs whose force-displacement relationship is quadratic. Both the spring sets satisfy the requirements derived in Section 3.2.3.

During the experiments the dead-band was measured for different levels of co-contraction by moving by hand the output joint within the actuator Range of Motion (RoM). The co-contraction level was controlled by setting equal absolute values for the internal torques of the agonist τ_{ϑ} and antagonist side τ_{ϑ^a}.

Table 2 shows the behavior of the dead-band for increasing level of co-contraction for the two sets. The quadratic set shows an increasing dead-band, which reaches the output joint RoM when the absolute value of the internal torques τ_{ϑ} and τ_{ϑ^a} is about 1.5Nm. On the contrary the optimized set of springs is effective in inverting the dead-band mechanical behavior. In particular, due to the numerical procedure adopted to compute the non-linear springs potential energy functional (see also Fiorio et al (2014)), we have a large dead-band for low levels of co-contraction.

Table 2 Behavior of the dead-band "DB" for the pnrVSA prototype with two different set of parallel and series non-linear springs.

Torque [Nm]	optimized set DB[deg]	quadratic set DB[deg]
0.12	104.61	3.50
0.25	100.81	27.90
0.50	87.73	69.90
1.00	61.62	85.50
1.50	49.81	entire RoM

5.2 Control simulations

We first tested the control law (8) on a simulation of the actuator represented in Figure 3. Springs were designed to comply to the conditions derived in Section 3.3 and therefore satisfy all the required conditions outlined in Section 3.2.3.

Figure 10 shows the results of applying (8) to the system. In particular, the plots (a), (b) and (c) shows the stiffness, the joint position and the sensitivity $\partial\hat{q}/\partial\hat{\tau}_{\vartheta^a}$ when we applied (8) with $v = 0$ and $u \neq 0$. In the plot (b) we can notice both the transient response (in blue) and the constant equilibrium configuration of the output joint (in red). The plots (d), (e) and (f), instead, show the results of applying (8) with the opposite choice of control parameters, i.e. $u = 0$ and $v \neq 0$. It is possible to notice that while the equilibrium configuration of the output joint changes, the stiffness remains constant.

Secondly, we tested the stochastic optimal control in Section 4.2. As depicted in Figure 11, in this case we simulated a two-DoF arm equipped with a pnrVSA at each joint. The arm was required to push against a wall with a constant force

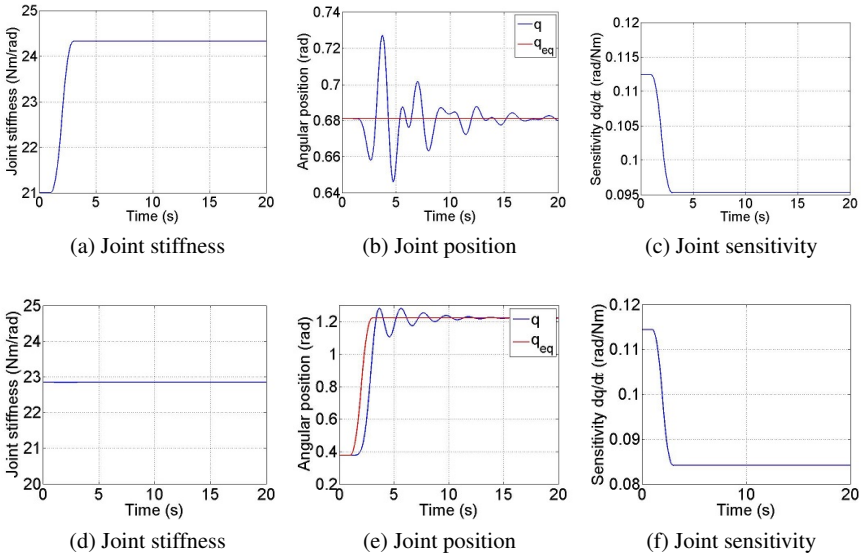

(a) Joint stiffness (b) Joint position (c) Joint sensitivity

(d) Joint stiffness (e) Joint position (f) Joint sensitivity

Fig. 10 Figures (a), (b) and (c) show the system response to the control law in Eq. (8) with $v = 0$ and $u \neq 0$. Figures (d), (e) and (f) show the system response to the same control action, but with the choice $u = 0$ and $v \neq 0$.

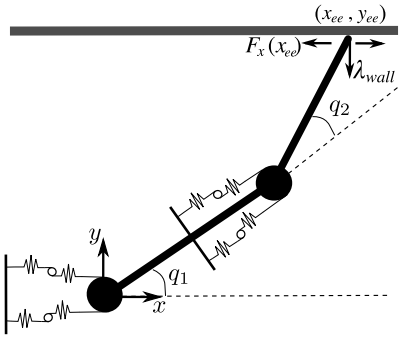

Fig. 11 Two-DOF manipulator equipped with two pnrVSAs. It is shown the pushing task against the wall together with the reaction force λ_{wall} and the divergent force field $F_x(x)$. Source (Berret et al (2013)).

while subject to an external disturbance chosen to be a divergent force field at the contact point. The control policy has been pre-computed with two different stiffness configuration: an high stiffness and a low stiffness configuration. The plots (a) and (b) of Figure 12 shows the x-coordinate of the end-effector during the application of the two control policies. The equilibrium configuration was required to be 0.3m. The stiffer solution, on the right, exhibits a lower error.

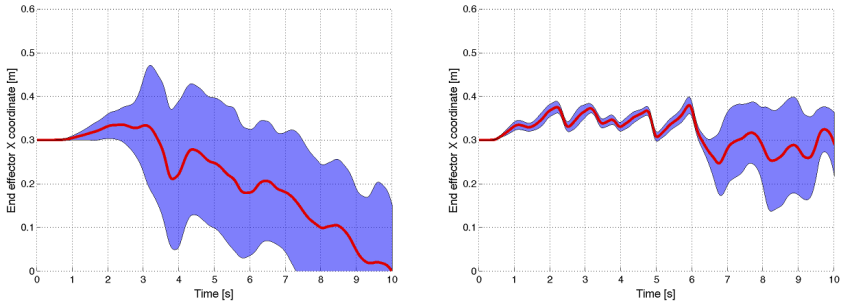

(a) pnrVSA - Low stiffness

(b) pnrVSA - High stiffness

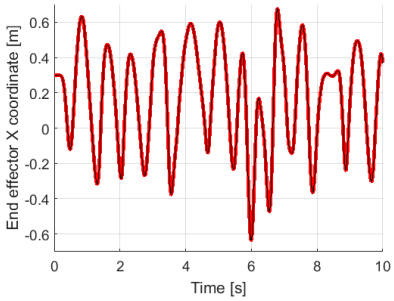

(c) VSA - High stiffness

Fig. 12 Figures (a) and (b) show the X-coordinate of the two-DoF arm end-effector when controlled with the SOC algorithm of Section 4.2. Plots show the average (red) and standard deviation (shaded blue) over 20 simulation trials. Figure (c) shows the behavior of the same two-DoF manipulator equipped with classical VSAs. Source (Romano et al (2014)).

Finally, we tested the stochastic optimal control algorithm with a two-DOF manipulator equipped with classical VSAs (without *pnr*). As shown in Figure 12 (c), the manipulator in this case is not able to maintain the desired position, neither for the high stiffness configuration.

The main result of the simulations is that the proposed actuator makes it possible to mimic some effects of muscle co-contraction in humans, which is useful to cope with noise and sensorimotor delays affecting physical/biological systems. The price to pay to achieve this behavior is a waste of energy associated with the need for stretching additional springs. This property is nevertheless similar to the large energy expenditure of muscle co-contraction and this moreover justifies the use of

optimal control techniques to reduce this energy consumption to a minimum. The fact that we stick to open-loop control laws is just to illustrate the properties of pn-rVSA for such an extreme case, but this does not prevent the use of feedback laws in real applications.

6 Conclusions and Future Work

This work presents the mechanical design of a novel actuator capable of actively changing its passive noise rejection characteristic. The proposed actuator is composed of two independent motors in an agonist-antagonist configuration and its design takes inspiration from the muscles configuration in biological systems. Crucial elements in the proposed system are four non-linear springs whose force-displacement characteristic has been customized for our specific needs.

The problem of quantifying analytically the effects and the propagation of internal static friction has been addressed and solved. Eventually, some important control properties of the novel variable stiffness actuator have been also characterized and tested in simulation. After a characterization of the system stiffness, we proposed a control action that guarantees a monotonically increasing joint stiffness, a desirable property for augmenting the system disturbance rejection. This property was guaranteed with minimal requirements on the spring potential energies (basically positiveness of the derivatives). We also showed how adding a planning element to the control (e.g. using SOC) can help attenuating external disturbances without explicitly relying on feedback.

The proposed actuator mimics a functional property of human antagonist muscle apparatus, but to make it more human-like, more work would be required. We aim in the next future at designing a new actuator to fully exploit the potential of our methodology. Future works include also the realization of a two degrees of freedom robotic arm actuated by three of these actuators: two acting on a single joint, one spanning two joints in a polyarticular-like configuration.

Appendix

6.1 Sensitivity Matrix Computation

Let's represent (2) in a compact way, with the following definition:

$$\begin{cases} -U_1'(\hat{\vartheta}) - U_2'(\hat{\vartheta} + \hat{q}) = \hat{\tau}_{\vartheta} \\ U_4'(\hat{\vartheta}^a) + U_3'(\hat{\vartheta}^a - \hat{q}) = \hat{\tau}_{\vartheta^a} \\ -U_2'(\hat{\vartheta} + \hat{q}) + U_3'(\hat{\vartheta}^a - \hat{q}) = \hat{\tau}_q \end{cases} \iff f(\alpha, \tau) = 0.$$

By resourcing to the implicit function theorem, the equation $f(\alpha,\tau)=0$ locally defines a function $\alpha(\tau)$ (equilibrium configuration) with sensitivity:

$$\frac{\partial \alpha}{\partial \tau} = -\left[\frac{\partial f}{\partial \alpha}\right]^{-1}\frac{\partial f}{\partial \tau}.$$

as easily follows by numerical derivation of the constrain equation $f(\alpha(\tau),\tau)=0$:

$$\frac{\partial f}{\partial \alpha}\frac{\partial \alpha}{\partial \tau}+\frac{\partial f}{\partial \tau}=0 \rightarrow \frac{\partial \alpha}{\partial \tau} = -\left[\frac{\partial f}{\partial \alpha}\right]^{-1}\frac{\partial f}{\partial \tau}.$$

Using the analytical expression of f given by (2), we obtain:

$$\frac{\partial f}{\partial \alpha} = \left[\frac{\partial f}{\partial \vartheta}\ \frac{\partial f}{\partial \vartheta^a}\ \frac{\partial f}{\partial \hat{q}}\right] = \begin{bmatrix} -U_1''-U_2'' & 0 & -U_2'' \\ 0 & U_4''+U_3'' & -U_3'' \\ -U_2'' & U_3'' & -U_2''-U_3'' \end{bmatrix},$$

and:

$$\frac{\partial f}{\partial \tau} = \begin{bmatrix} -1 & 0 & 0 \\ 0 & -1 & 0 \\ 0 & 0 & -1 \end{bmatrix}$$

which eventually results in the following expression:

$$\frac{\partial \alpha}{\partial \tau} = \begin{bmatrix} -U_1''-U_2'' & 0 & -U_2'' \\ 0 & U_4''+U_3'' & -U_3'' \\ -U_2'' & U_3'' & -U_2''-U_3'' \end{bmatrix}^{-1}$$

$$\frac{\partial \alpha}{\partial \tau} = \begin{bmatrix} \frac{\partial \hat{\vartheta}}{\partial \hat{\tau}_\vartheta} & \frac{\partial \hat{\vartheta}}{\partial \hat{\tau}_\vartheta^a} & \frac{\partial \hat{\vartheta}}{\partial \hat{\tau}_q} \\ \frac{\partial \hat{\vartheta}^a}{\partial \hat{\tau}_\vartheta} & \frac{\partial \hat{\vartheta}^a}{\partial \hat{\tau}_\vartheta^a} & \frac{\partial \hat{\vartheta}^a}{\partial \hat{\tau}_q} \\ \frac{\partial \hat{q}}{\partial \hat{\tau}_\vartheta} & \frac{\partial \hat{q}}{\partial \hat{\tau}_\vartheta^a} & \frac{\partial \hat{q}}{\partial \hat{\tau}_q} \end{bmatrix} =$$

$$\begin{bmatrix} -(U_2''U_3''+U_2''U_4''+U_3''U_4'') & -U_2''U_3'' & U_2''(U_3''+U_4'') \\ U_2''U_3'' & U_1''U_2''+U_1''U_3''+U_2''U_3'' & -U_3''(U_1''+U_2'') \\ U_2''(U_3''+U_4'') & U_3''(U_1''+U_2'') & -(U_1''+U_2'')(U_3''+U_4'') \end{bmatrix}$$

$$\cdot \frac{1}{U_1''U_2''U_3''+U_1''U_2''U_4''+U_1''U_3''U_4''+U_2''U_3''U_4''}$$

6.2 Actuator specifications

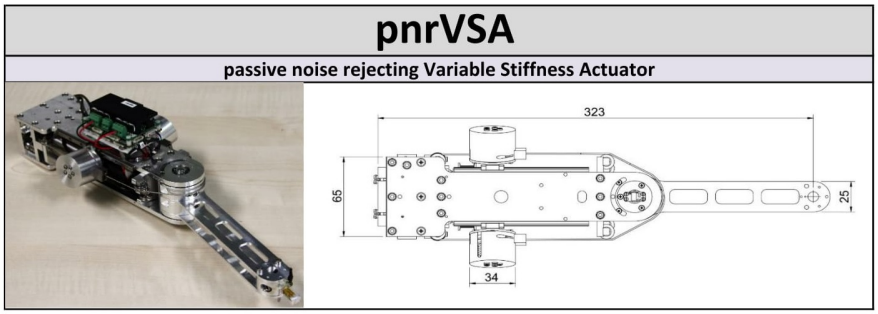

Operating Data				
#	(quantity)		(unit)	(value)
Mechanical				
1	Continuous Output Power		[W]	23
2	Nominal Torque		[Nm]	1
3	Nominal Speed		[rad/s]	16.82
4	Nominal Stiffness Variation Time	with no load	[s]	0.2
5		with nominal torque	[s]	0.2
6	Peak (Maximum) Torque		[Nm]	5.15
7	Maximum Speed		[rad/s]	17.94
8	Maximum Stiffness		[Nm/rad]	11.92
9	Minimum Stiffness		[Nm/rad]	0
10	Maximum Elastic Energy		[J]	1.7
12	Maximum deflection	with max stiffness	[°]	60
13		with min stiffness	[°]	60
14	Active Rotation Angle		[°]	+/-120
15	Angular Resolution		[°]	0.032
16	Weight		[Kg]	0.65
Electrical				
17	Nominal Voltage		[V]	48
18	Nominal Current		[A]	1
19	Maximum Current		[A]	4
Control				
20	Voltage Supply		[V]	48
21	Nominal Current		[A]	0.06
22	I/O Protocol		[]	CAN

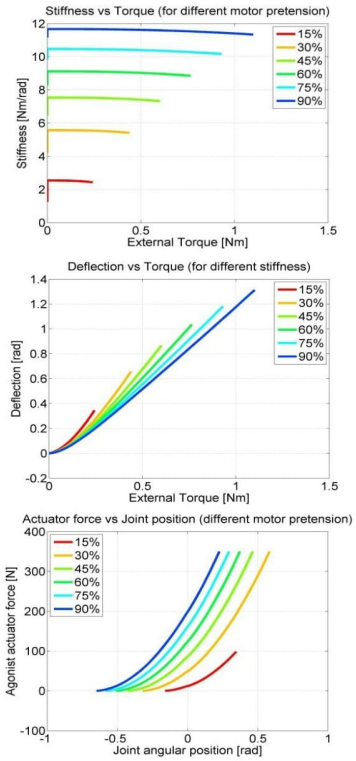

Fig. 13 The VIACTORS VSA datasheet of the pnrVSA. In the plots on the right hand side we report the pnrVSA characteristic curves for different internal motor pretensions. This pretension has to be interpreted as the applied torque at motor capstan, ranging from 15 to 90 percent of the stall torque. The VIACTORS Variable Stiffness Joint Datasheet was developed within the VIACTORS project, which is a part of the EU 7th Framework Programme. Source (Fiorio et al (2012)).

References

Albu-Schaffer A, Hirzinger G (2002) Cartesian impedance control techniques for torque controlled light-weight robots. In: Robotics and Automation, 2002. Proceedings. ICRA '02. IEEE International Conference on, vol 1, pp 657–663 vol.1, DOI 10.1109/ROBOT.2002.1013433

Armstrong B (1988) Dynamics for robot control: Friction modelling and ensuring excitation during parameter identification. In: Dissertation, Stanford University

Berret B, Ivaldi S, Nori F, Sandini G (2011) Stochastic optimal control with variable impedance manipulators in presence of uncertainties and delayed feedback. In: International Conference on Intelligent Robots and Systems (IROS2011), IEEE, pp 4354–4359

Berret B, Sandini G, Nori F (2012) Design principles for muscle-like variable impedance actuators with noise rejection property via co-contraction. In: Humanoid Robots (Humanoids), 2012 12th IEEE-RAS International Conference on, pp 222–227, DOI 10.1109/HUMANOIDS.2012.6651524

Berret B, Yung I, Nori F (2013) Open-loop stochastic optimal control of a passive noise-rejection variable stiffness actuator: Application to unstable tasks. In: 2013 IEEE/RSJ International Conference on Intelligent Robots and Systems, pp 3029–3034, DOI 10.1109/IROS.2013.6696785

Bicchi A, Tonietti G, Piaggio E (2002) Design, realization and control of soft robot arms for intrinsically safe interaction with humans. In: Proc. IARP/RAS Workshop on Technical Challenges for Dependable Robots in Human Environments, pp 79–87

Bona B, Indri M (2005) Friction compensation in robotics: an overview. In: Decision and Control, 2005 and 2005 European Control Conference. CDC-ECC '05. 44th IEEE Conference on, pp 4360–4367, DOI 10.1109/CDC.2005.1582848

Burdet E, Osu R, Franklin DW, Milner TE, Kawato M (2001a) The central nervous system stabilizes unstable dynamics by learning optimal impedance. Nature 414(6862):446–9, DOI 10.1038/35106566

Burdet E, Osu R, Franklin DW, Milner TE, Kawato M (2001b) The central nervous system stabilizes unstable dynamics by learning optimal impedance. Nature 414(6862):446–449, DOI 10.1038/35106566

De Luca CJ, Mambrito B (1987) Voluntary control of motor units in human antagonist muscles: coactivation and reciprocal activation. Journal of Neurophysiology 58(3):525–542, URL http://jn.physiology.org/content/58/3/525, http://jn.physiology.org/content/58/3/525.full.pdf

Del Prete A, Nori F, Metta G, Natale L (2012) Control of Contact Forces: the Role of Tactile Feedback for Contact Localization. In: Intelligent Robots and Systems (IROS), 2012 IEEE/RSJ International Conference on

Eiberger O, Haddadin S, Weis M, Albu-Sch äffer A, Hirzinger G (2010) On joint design with intrinsic variable compliance: Derivation of the dlr qa-joint pp 1687 – 1694

Fiorio L, Parmiggiani A, Berret B, Sandini G, Nori F (2012) pnrvsa: human-like actuator with non-linear springs in agonist-antagonist configuration

Fiorio L, Romano F, Parmiggiani A, Sandini G, Nori F (2013) On the effects of internal stiction in pnrvia actuators. In: Humanoid Robots (Humanoids), 2013 13th IEEE-RAS International Conference on, pp 362–367, DOI 10.1109/HUMANOIDS.2013.7030000

Fiorio L, Romano F, Parmiggiani A, Sandini G, Nori F (2014) Stiction compensation in agonist-antagonist variable stiffness actuators. In: Proceedings of Robotics: Science and Systems, Berkeley, USA

Fumagalli M, Ivaldi S, Randazzo M, Natale L, Metta G, Sandini G, Nori F (2012) Force feedback exploiting tactile and proximal force/torque sensing. Theory and implementation on the humanoid robot iCub. Autonomous Robots 33(4):381–398

Hill A, Gasser H (1924) The dynamics of muscular contraction

Hogan N (1984) Adaptive control of mechanical impedance by coactivation of antagonist muscles. Automatic Control, IEEE Transactions on 29(8):681–690, DOI 10.1109/TAC.1984.1103644

Kappen HJ (2011) Optimal control theory and the linear Bellman equation, Cambridge University Press, p 363387. DOI 10.1017/CBO9780511984679.018

McMahon T (1984) Muscle, Reflexes, and Locomotion

Migliore SA, Brown EA, DeWeerth SP (2005) Biologically inspired joint stiffness control. In: Proceedings of the 2005 IEEE International Conference on Robotics and Automation, ICRA 2005, April 18-22, 2005, Barcelona, Spain, pp 4508–4513, DOI 10.1109/ROBOT.2005.1570814

Nori F, Berret B, Fiorio L, Parmiggiani A, Sandini G (2012) Control of a single degree of freedom noise rejecting-variable impedance. In: Proceedings of the 10th international IFAC symposium on Robot Control (SYROCO2012)

Paillard J (1996) Fast and slow feedback loops for the visual correction of spatial errors in a pointing task: a reappraisal. Can J Physiol Pharmacol 74:401–417

Parra-Vega V, Arimoto S (1996) A passivity based adaptive sliding mode position-force control for robot manipulators. In: International Journal of Adaptive Control and Signal Processing, pp 365–377

Petit F, Chalon M, Friedl W, Grebenstein M, Albu-Schäffer A, Hirzinger G (2010) Bidirectional antagonistic variable stiffness actuation: Analysis, design & implementation. In: ICRA, pp 4189–4196

Polit A, Bizzi E (1979) Characteristics of motor programs underlying arm movements in monkeys. Journal of Neurophysiology 42(1):183–194

Pratt G, Williamson M (1995) Series elastic actuators. In: Intelligent Robots and Systems 95. 'Human Robot Interaction and Cooperative Robots', Proceedings. 1995 IEEE/RSJ International Conference on, vol 1, pp 399–406 vol.1

Romano F, Fiorio L, Sandini G, Nori F (2014) Control of a two-dof manipulator equipped with a pnr-variable stiffness actuator. In: Intelligent Control (ISIC), 2014 IEEE International Symposium on, pp 1354–1359, DOI 10.1109/ISIC.2014.6967620

Schiavi R, Grioli G, Sen S, Bicchi A (2008) Vsa-ii: a novel prototype of variable stiffness actuator for safe and performing robots interacting with humans. In: Robotics and Automation, 2008. ICRA 2008. IEEE International Conference on, pp 2171–2176, DOI 10.1109/ROBOT.2008.4543528

Theodorou E, Buchli J, Schaal S (2010) A generalized path integral control approach to reinforcement learning. Journal of Machine Learning Research 11(Nov):3137–3181

Tomei P (2000) Robust adaptive friction compensation for tracking control of robot manipulators. IEEE Trans Automat Contr 45(11):2164–2169

Tonietti G, Schiavi R, Bicchi A (2005) Design and control of a variable stiffness actuator for safe and fast physical human/robot interaction. In: ICRA, IEEE, pp 526–531

Traversaro S, Pucci D, Nori F (2015) In situ calibration of six-axis force-torque sensors using accelerometer measurements. In: 2015 IEEE International Conference on Robotics and Automation (ICRA), IEEE, pp 2111–2116

Van Ham R, G Sugar T, Vanderborght B, WHollander K, Lefeber D (2009) Compliant actuator designs. Robotics & Automation Magazine, IEEE pp 16 81–94

Vanderborght B, Albu-Sch äffer A, Bicchi A, Burdet E, Caldwell DG, Carloni R, Catalano MG, Eiberger O, Friedl W, Ganesh G, Garabini M, Grebenstein M, Grioli G, Haddadin S, Hoppner H, Jafari A, Laffranchi M, Lefeber D, Petit F, Stramigioli S, Tsagarakis NG, Damme MV, Ham RV, Visser LC, Wolf S (2013) Variable impedance actuators: A review. Robotics and Autonomous Systems 61(12):1601–1614

Vitiello N, Cattin E, Roccella S, Giovacchini F, Vecchi F, Carrozza MC, Dario P (2007) The neurarm: towards a platform for joint neuroscience experiments on human motion control theories. In: 2007 IEEE/RSJ International Conference on Intelligent Robots and Systems, IEEE, pp 1852–1857

de Wit CC, Olsson H, Astrom K, Lischinsky P (1994) A new model for control of systems with friction. In: IEEE Trans. on Automatic Control, vol 40, pp 419–425